Reptation and Beyond: Neutron Spin Echo Experiments Verify the Fundamental Predictions of the Cooperative-Dynamics Generalized Langevin Equation Theory

Margarita Kruteva,[1] Jürgen Allgaier,[1] Marina Guenza,[2] Rustem Valiullin,[3] Ingo Hoffmann,[4] and Dieter Richter[1]
[1]Jülich Centre for Neutron Science, Forschungszentrum Jülich GmbH, 52428 Jülich, Germany
[2]Department of Chemistry and Biochemistry, University of Oregon, Eugene, Oregon 97403, USA
[3]Felix Bloch Institute for Solid State Physics, Leipzig University, Leipzig, 04103 Germany
[4]Institut Laue-Langevin (ILL), 71 avenue des Martyrs, 38000 Grenoble, France

(Received 28 January 2026; accepted 29 May 2026; published 13 July 2026; corrected 17 July 2026)

We have investigated the dynamics of nonentangled and weakly entangled polyisoprene (PI) melts using neutron spin echo spectroscopy and pulsed field gradient NMR and compared the spectra with those from a highly entangled PI melt. Except for Brownian diffusion, which was observed in the long-time regime using NMR, the spectra from nonentangled and weakly entangled PI chains were identical. Dividing out Brownian diffusion, these reduced spectra also quantitatively agree with those from the highly entangled PI melt. Reevaluating the results for poly(butylene oxide) leads to an identical observation, indicating universality. These experiments provide quantitative proof of key predictions of theory: (i) the correlation hole potential governs both the subdiffusivity of nonentangled systems and the cooperative dynamics within the entanglement volume, and (ii) as the spectra from a weakly entangled PI melt also coincide with those from the shorter and highly entangled PI, the entanglement potential, which creates topological constraints, acts in the same way for weakly and strongly entangled melts.

DOI: 10.1103/9n96-whkp

Introduction—In the case of high-molecular-weight polymer melts, chain interpenetration leads to topological constraints that dominate dynamics at all scales, from the mesoscopic to the macroscopic level of rheology. These constraints have been described with great success in terms of the phenomenological tube model by Doi and Edwards [1] and De Gennes [2]. In this model, the action of the interpenetrating chains on tagged chains is approximated by a mesoscopic tube along its profile that restricts lateral motion; the parameter is the step length that equals the diameter of the confining tube. If semiflexibility is accounted for, the dynamics of short chains can be accurately modeled using the Rouse model [3], which assumes that the chain is in a heat bath and is subject to entropic restoring forces. While both theories can describe highly entangled and unentangled melts, they cannot describe weakly entangled polymer melts.

More recently, fundamental microscopic theories have been proposed. Using mode coupling theory, Schweizer *et al.* discussed the dynamics of a tagged chain in relation to the other chains present [4–7]. Guenza extended this framework by explicitly accounting for the cooperative motion of groups of polymer chains interacting via an effective pair potential, leading to the formulation of the cooperative-dynamics generalized Langevin equation (CDGLE). The CDGLE describes the collective motion of interacting polymer chains mediated by the correlation-hole pair potential. Within this formulation, the dynamics naturally decomposes into collective and relative modes, from which the effective single-chain motion can be systematically reconstructed [8–11]. Explicit consideration of a pair of chains within the correlation hole enabled both a correlation hole potential of mean force and an entanglement potential, which restricts the relative motion of chain segments beyond a distance characterized by the tube diameter. Entanglements are viewed as dynamical constraints on monomer diffusion that emerge collectively from topological restrictions rather than as a static barrier. The model captures the chain dynamics in the crossover regime and reproduces neutron spin echo (NSE) spectra for polyethylene melts up to $Z = 12$, where Z denotes the number of entanglements per chain [10].

Richter and coworkers also studied the dynamics of short tracers in strongly entangled poly(ethylene oxide) (PEO) melts [12]. Regardless of the tracer's molecular weight, they found that the dynamics were strongly affected by the host dynamics; the evolving cooperative motion was restricted by the entanglement volume. Very recently we studied weakly entangled PBO and obtained an unexpected result. The PBO spectra, when divided by those from highly entangled PBO, equaled the spectra expected from Brownian diffusion, as determined by pulsed field gradient (PFG) NMR [13].

Bearing this in mind, we investigated several nonentangled and weakly-entangled polyisoprene (PI) melts, comparing their spectra with those of highly entangled PI. The following results stand out: (i) except for Brownian diffusion, which is observed in the long-time regime by PFG-NMR, the spectra of different short nonentangled and weakly entangled PI chains are identical; (ii) dividing out Brownian diffusion, these reduced spectra also quantitatively agree with those from the highly entangled PI melt, where the spectra originate from the dynamics within the entanglement tube; and (iii) a similar observation for PBO demonstrates universality. These experimental observations strongly support the predictions of the CDGLE, as developed by Guenza [10].

Theoretical—

CDGLE theory: The novelty of the CDGLE lies in its description of the diffusive dynamics of a collectively correlated group of polymer chains, initially coupled through the correlation-hole pair potential. By constructing appropriate linear combinations of relative and collective modes, the theory yields the effective single-chain dynamics, which naturally exhibits subdiffusive center-of-mass motion arising from dynamical correlations with the interpenetrating chains. The correlation-hole pair potential between the centers of mass of interacting polymers is obtained by projecting the underlying monomer-monomer interactions onto the corresponding center-of-mass coordinates [8]. For a more detailed description see the Supplemental Material [14]. The number of dynamically correlated chains scales as the square root of the number of chain segments, corresponding to the number of polymers that statistically interpenetrate a given chain. The entanglement potential acts on the relative chain motion and is zero for distances smaller than the tube diameter, d increasing beyond this value, where d is a theoretical parameter. The correlation-hole potential is isotropic and local, and its functional form is applied uniformly across all polymer samples considered. As Guenza has demonstrated, this theory can accurately describe NSE spectra for polyethylene (PE) up to $Z = 12$ [10].

Subdiffusivity relates to the dynamics of center-of-mass coordinates, which are affected by the correlation-hole potential. This is also evident for chains shorter than the entanglement length. For longer chains, cooperative motion is confined within the reptation tube and only exhibits subdiffusive behavior on a local scale. A detailed comparison with NSE spectra from PE revealed the following: (i) for a short chain (one entanglement), the contribution of the entanglement potential is weak yet discernible; and (ii) for a chain with two entanglements, the entanglement potential significantly affects the spectra. A comparison with the Rouse model shows that it fails to reproduce the data even at short times, which is expected given that the Rouse model is formally valid only for fully flexible chains. By contrast, adopting a freely rotating chain description for polyethylene, using the polymer's characteristic ratio, dramatically improves the accuracy of the short-time dynamics, where correlated center-of-mass motion is already accounted for [22]. It is important to note that both the center-of-mass correlation-hole potential and the monomer confining potential are included in the theoretical framework used to describe polymer melt dynamics, independently of chain length (unentangled, entangled, or strongly entangled). For short chains, however, diffusion occurs on a timescale shorter than that required for the entanglement potential to become dominant, rendering its effect negligible in practice. For longer chains, the cooperative dynamics of the correlation hole potential align well with the spectra

TABLE 1. Achieved PI materials and their characterization (GPC-LS): M_n and M_w—number averaged and weight averaged molecular weights; M_w/M_n polydispersity; N—monomer number.

	M_n	M_w/M_n	N
hPI6k	5560	1.06	87
hPI9k	9490	1.01	141
hPI12k	11 800	1.01	175
dPI6k	6180	1.01	83
dPI9k	10 800	1.02	145
dPI12k	12 100	1.02	162
hPI350K	304 000	1.01	4515
dPI350K	350 000	1.03	4743

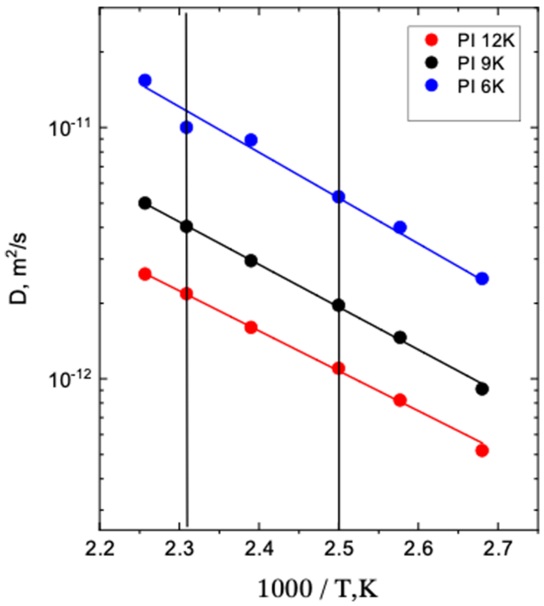

FIG. 1. The Brownian diffusion coefficients of different PIs in their melts as obtained using PFG-NMR. The vertical lines display the temperatures, where the NSE experiments took place.

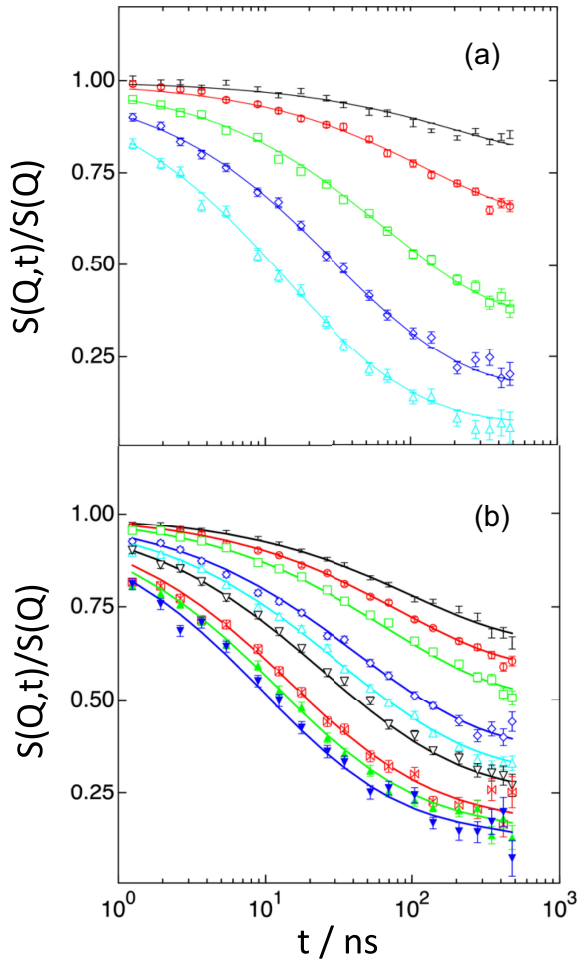

FIG. 2. PI350K spectra: (a) at 400 K, taking the middle stripes from the detector; Q values from above are 0.052, 0.072, 0.103, 0.134, 0.166 Å^{-1}; (b) at 433 K presenting all detector stripes. Q values from above are 0.065, 0.072, 0.80, 0.095, 0.103, 0.111, 0.127, 0.134, 0.142 Å^{-1}; lines: see text.

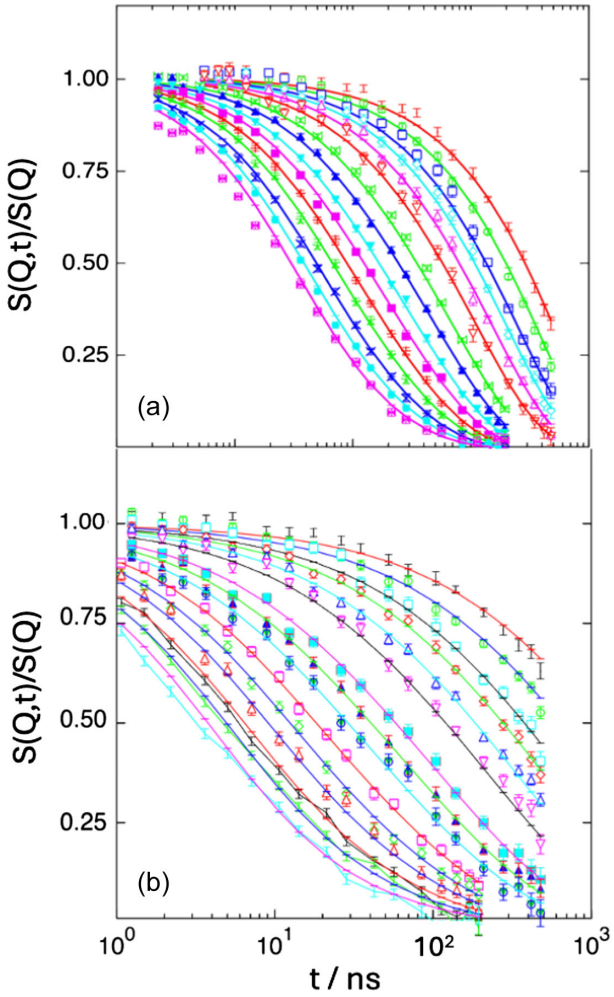

FIG. 3. (a) PI6K (b) PI12K spectra at 433K; Q values from above: 0.045; 0.052, 0.060, 0.065, 0.072, 0.080, 0.095, 0.103, 0.111, 0.123, 0.134, 0.144, 0.156, 0.166, 0.177 Å^{-1}; lines see text.

at short times. At longer times, however, the entanglement potential also needs to be considered.

Dynamic structure factor: Neutron scattering provides direct access to polymer dynamics and structure at the level of the chains. In this Letter, we studied the dynamics of a labeled chain within the melt, which gives rise to coherent scattering that monitors the monomer-monomer pair correlation function within this chain [23]. In terms of the Gaussian approximation for the intermediate scattering function, we obtain

$$S(Q,t) = \frac{1}{N}\sum_{n,m}^{N} \exp\left\{-\frac{Q^2}{6}\left\langle (r_m(t) - r_n(0))^2 \right\rangle\right\}. \quad (1)$$

The sum runs over all segments m and n at times $t = 0$ and t within the labeled chain. Q is the momentum transfer, and N is the number of monomers or segments within the chain. In terms of the CDGLE, both the normal modes of relative motion and those of cooperative motion contribute to the average square displacement, $\langle (r_m(t) - r_n(0))^2 \rangle$ and are thus sensitive to both. The details of the considered dynamic structure factor are presented in the Supplemental Material [14].

Experiments—

Synthesis and characterization: Nearly monodisperse hydrogenous and deuterated linear PI of various molecular weights were synthesized by anionic polymerization. The characterization of the sample measured by gel permeation chromatography (GPC) and light scattering (LS) is listed in Table 1.

PFG-NMR diffusion measurements: For the details of the PFG-NMR experiments see the Supplemental Material [14]. To compare the NSE results with direct measurements of Brownian diffusion on the micrometer scale, PFG-NMR experiments were performed on the PI samples investigated by NSE. To obtain higher precision, the temperature dependence of the diffusion coefficients was measured and interpolated using an Arrhenius law in each case. Figure 1 displays the results for PI6K, PI9K, and PI12K.

TABLE 2. Parameters for PI350K obtained from a fit with $S(Q,t)$ (see the Supplemental Material [14]); N_e number of monomers in an entanglement strand; Wl4 Rouse rate; α_0 strength of NG; $t_{\max}$ and t_w maximum time and width of the log normal distribution describing the NG. χ^2 is a mean squared deviation. For the parameters $t_{\max}$ and t_w the values were fixed (f).

T [K]	N_e [27]	Wl4 [Å^4/ns]	α_0	$t_{\max}$ [ns]	t_w [ns]	χ^2
400 K	132 ± 3	5613 ± 61	0.0091 ± 0.005	300.0 f	2.0 f	2.19
433 K	135 ± 2.2	$11\,821 \pm 112$	0.103 ± 0.004	150 f	2.0 f	1.44

NSE experiments: Our study was performed on IN15 applying neutron wavelengths of 10 Å and 13.5 Å respectively providing an experimental time window 0.2 ns $< t <$ 500 ns [24]. For all samples Q values 0.052, 0.072, 0.103, 0.134, and 0.166 Å^{-1} were studied. The Q values relate to the center stripes of the detector; in each case the off-center stripes offered another 10 Q-values, even though the resolution was lower [25].

The spectra were corrected for resolution and background. As the background did not reveal any structure, time-averaged constants were subtracted. Figure 2 shows the spectra obtained from the PI350K sample at 400 K and 433 K. Figure S3 (see the Supplemental Material [14]) compares the new PI350K data with a measurement taken seven years ago. This complete agreement demonstrates the stability of the IN15 instrument.

The spectra on PI6K and PI12K taken at 400 K and PI9K at 433K are shown in the Supplemental Material [14], and Fig. 3 present spectra taken from the PI6K, PI12K melts at 433K.

Modeling of the spectra: Starting with the high-molecular weight melt, we now model the results from the different melts. As the PI350K sample is highly entangled, we describe the spectra in terms of the dynamic structure factor $S(Q,t)$ as described by Monkenbusch *et al.* [26]. The approach is based on De Gennes's local reptation ideas [2] and extends the method to include the relaxation of the Rouse blob within the tube, as well as the non-Gaussian (NG) dynamics of the Rouse blob (see the Supplemental Material [14]). The strength of the non-Gaussianity is determined by parameter; α_0; the time where the logarithmic Gaussian function describing the time dependence of NG assumes its maximum and the width of this function are $t_{\max}$ and t_w. $t_{\max}$ should roughly correspond to the Rouse time of the Rouse blob. The lines in Fig. 2 display the fit of the PI350K data at both temperatures, and Table 2 presents the achieved fitting parameters.

Prior knowledge is important for modeling short chain melts. For the center of mass diffusion, we use the results from the PFG-NMR measurements (Fig. 1). For the Rouse rates, we use Wl4, which was obtained by fitting the PI350K spectra. The fitting parameters were the subdiffusion exponent ν, the crossover mean-squared displacement (MSD) r^2_{cross}, and the NG strength α_0. As can be seen in Figs. 3 and S3–S5 [14], the quality of the fits was always excellent. Table 3 presents the obtained parameters.

The presented fits to the short PI chains accurately describe the NSE spectra. We note that in all cases the crossover distance from subdiffusive to Brownian diffusion is found between R_e and R_g.

Discussion—In the CDGLE theory, two interchain potentials act on the motion of the polymer chains: the correlation hole potential and the entanglement potential. In entangled melts, the dynamical correlations generated by the correlation-hole potential, which are present in all samples, become spatially limited by topological constraints in entangled systems. The potential itself retains the same functional form across all degrees of polymerization.

TABLE 3. Parameters for shorter chains obtained from a fit with $S(Q,t)$ (Supplemental Material [14]); D: Brownian diffusion coefficient from PFG-NMR; $\sqrt{r^2_{\text{cross}}}$, distance, where the subdiffusive com MSD crosses over to Brownian diffusion; ν, exponent characterizing the subdiffusivity; R_e and R_g, end to end distance and radius of gyration of the different polymers; α_0, strength of NG.

Polymer	T [K]	D[Å^2/ns]	ν	$\sqrt{r^2_{\text{cross}}}$[Å]	R_e[Å]	R_g[Å]	α_0
PI6K	433	1.0 f	0.76 ± 0.005	54 ± 1	64	26	0.31 ± 0.01
PI9K	433	0.40 f	0.66 ± 0.004	46 ± 2	82	33	0.23 ± 0.015
PI12K	433	0.22 f	0.66 ± 0.004	58 ± 1	91	37	0.19 ± 0.007
PI6K	400	0.5 f	0.75 ± 0.003	62 ± 2	64	26	0.413 ± 0.014
PI12K	400	0.11 f	0.64 ± 0.006	74 ± 4	91	37	0.29 ± 0.017

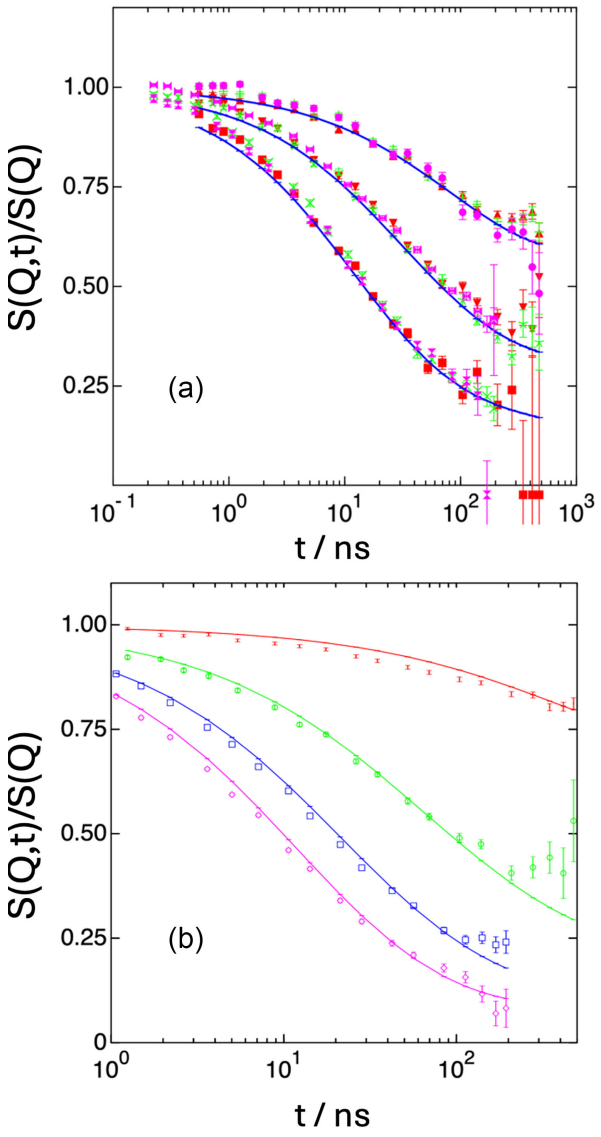

FIG. 4. (a) Comparison of the reduced melt spectra from PI6K (magenta), PI9K (green), PI12K (red) with the spectra from PI350K (blue lines); Q values from above: 0.071, 0.103, 0.132 Å^{-1}; error bars: statistical errors only. (b) reduced spectra from PBO12K at 415K compared to the spectra from PBO200K (solid lines). The colors for the data points correspond to the associated lines. Q values from above: 0.047, 0.096, 0.129, 0.151 Å^{-1}.

Therefore, if we divide the spectra by their respective Brownian diffusion contributions, $S_{\mathrm{diff}}(Q,t) = \exp[-Q^2 Dt]$ obtained from PFG-NMR on the micrometer scale, the such reduced spectra should (i) form a master curve representing the action of the two potentials, and (ii) agree with the spectra from the high-M_w PI350K sample, where the spectra originate from the dynamics within the entanglement tube.

The PI350K results are only available in the range 0.065 Å^{-1} $< Q <$ 0.144 Å^{-1}, which makes it impossible to compare the lowest Q. Figure 4(a) shows a comparison of the PI350K spectra (lines) with the reduced spectra from the PI12K, PI9K, and PI6K melts. Where no error is indicated, the error bars are smaller than the symbol sizes. The detector averages were taken for the comparison. As can be seen, the reduced spectra from the low molecular weight materials quantitatively agree with each other and with those taken at high molecular weight.

Next, we will investigate the universality of this result and evaluate the recently published poly(butylene oxide) (PBO) results using a similar approach [13]. While PI is hydrophobic, the oxygen-containing PBO is largely hydrophilic. Once again, we observe good agreement between the reduced PBO12K spectra and those from PBO200K [Fig. 4(b)]. The slight deviation observed for long times in both PI and PBO spectra at higher Q relates to systematic errors that commonly occur when evaluating NSE raw data, if the echo is below about 5%. This is the case for the original low M_w PI and PBO spectra.

Conclusions—Phenomenologically, the complex dynamics of polymer melts are described by the tube theory. Based on correlation-hole and entanglement potentials, the CDGLE theory offers a fundamental understanding. We investigated its key predictions: the action of two potentials and their domain of relevance. Except for Brownian diffusion, we observed that the spectra from nonentangled and weakly entangled melts are identical and coincide with those of highly entangled melts. The chains move under the action of potentials that are quantitatively valid for all these melts, ranging from subdiffusivity in nonentangled systems to cooperative dynamics within the entanglement volume.

The experimental results quantitatively prove the CDGLE prediction that the correlation hole potential governs the subdiffusivity of nonentangled systems, as well as the cooperative dynamics within the entanglement volume. As the spectra from the weakly entangled PI12K coincide with those of the shorter PI and the highly entangled PI, it appears that the entanglement potential, which creates topological constraints, acts in the same way for weakly and strongly entangled melts. This conclusion also holds for hydrophilic PBO.

The present experiments reveal a simple organizing principle in polymer melt dynamics: once Brownian diffusion is removed, nonentangled, weakly entangled, and highly entangled chains exhibit the same reduced NSE spectra. This collapse shows that short-chain subdiffusion and motion within the entanglement volume are governed by common microscopic interactions, rather than by separate dynamical mechanisms. CDGLE provides a theoretical framework for this observation by linking the spectra to correlation-hole-mediated cooperative dynamics and entanglement constraints. The agreement between chemically distinct PI and PBO melts further suggests that this mechanism reflects a general property of dense macromolecular liquids. More broadly, cooperative subdiffusion is emerging across soft-matter and biological systems, including protein condensates, where molecular motion is shaped by correlations

with the surrounding macromolecular environment. The experimentally established connection between microscopic interactions and reduced spectra can guide future neutron-scattering experiments, coarse-grained simulations, and predictive models of diffusion, relaxation, and viscoelasticity.

Acknowledgments—We acknowledge Institute Laue Langevin for granting the neutron beamtime (Experiment 9-11-2148). M. G. G. acknowledges support from the National Science Foundation under Grant No. CHE-2154999.

Data availability—The data that support the findings of this article are openly available [24]; embargo periods may apply.

[1] M. Doi and S. F. Edwards, *The Theory of Polymer Dynamics* (Clarendon press Oxford, Oxford, 1986).
[2] P. G. de Gennes, Reptation of a polymer chain in the presence of fixed obstacles, J. Chem. Phys. **55**, 572 (1971).
[3] P. E. Rouse, A theory of the linear viscoelastic properties of dilute solutions of coiling polymers, J. Chem. Phys. **21**, 1272 (1953).
[4] K. S. Schweizer, Mode-coupling theory of the dynamics of polymer liquids: Qualitative predictions for flexible chain and ring melts, J. Chem. Phys. **91**, 5822 (1989).
[5] K. S. Schweizer, Mode-coupling theory of the dynamics of polymer liquids, J. Non. Cryst. Solids **131**, 643 (1991).
[6] K. S. Schweizer and G. Szamel, Crossover to entangled dynamics in polymer solutions and melts, J. Chem. Phys. **103**, 1934 (1995).
[7] G. Szamel and K. S. Schweizer, Reptation as a dynamic mean-field theory: Self and tracer diffusion in a simple model of rodlike polymers, J. Chem. Phys. **100**, 3127 (1994).
[8] M. Guenza, Many chain correlated dynamics in polymer fluids, J. Chem. Phys. **110**, 7574 (1999).
[9] M. Guenza, Cooperative dynamics in unentangled polymer fluids, Phys. Rev. Lett. **88**, 025901 (2001).
[10] M. G. Guenza, Cooperative polymer dynamics at the crossover between the unentangled and the entangled regimes: Theoretical predictions of scattering and linear shear relaxation for polyethylene melts, Macromolecules **57**, 9651 (2024).
[11] M. G. Guenza, Localization of chain dynamics in entangled polymer melts, Phys. Rev. E **89**, 052603 (2014).
[12] M. Kruteva, M. Zamponi, I. Hoffmann, J. Allgaier, M. Monkenbusch, and D. Richter, Non-Gaussian and cooperative dynamics of entanglement strands in polymer melts, Macromolecules **54**, 11384 (2021).
[13] M. Kruteva, J. Allgaier, M. Monkenbusch, R. Valiullin, I. Hoffmann, and D. Richter, Cooperative dynamics of highly entangled linear polymers within the entanglement tube, ACS Macro Lett. **13**, 335 (2024).
[14] See Supplemental Material at http://link.aps.org/supplemental/10.1103/9n96-whkp for synthesis details, calculations of the dynamic structure factor, CDGLE theory, PFG NMR measurements, NSE results for PI350K, PI6K and PI12K at 400K, fit of NSE spectra from PI6K with Rouse model, which Includes Refs. [15–21].
[15] A. Sharma, M. Kruteva, J. Allgaier, I. Hoffmann, P. Falus, M. Monkenbusch, and D. Richter, Chain confinement and anomalous diffusion in the cross over regime between rouse and reptation, ACS Macro Lett. **11**, 1343 (2022).
[16] P. G. De Gennes, Coherent scattering by one reptating chain, J. Phys. (Orsay, France) **42**, 735 (1981).
[17] D. Richter, B. Farago, L. J. Fetters, J. S. Huang, B. Ewen, and C. Lartigue, Direct microscopic observation of the entanglement distance in a polymer melt, Phys. Rev. Lett. **64**, 1389 (1990).
[18] R. Butera, L. J. Fetters, J. S. Huang, D. Richter, W. Pyckhout-Hintzen, A. Zirkel, B. Farago, and B. Ewen, Microscopic and macroscopic evaluation of fundamental facets of the entanglement concept, Phys. Rev. Lett. **66**, 2088 (1991).
[19] D. Richter, R. Butera, L. J. Fetters, J. S. Huang, B. Farago, and B. Ewen, Entanglement constraints in polymer melts. A neutron spin echo study, Macromolecules **25**, 6156 (1992).
[20] M. Zamponi, M. Kruteva, M. Monkenbusch, L. Willner, A. Wischnewski, I. Hoffmann, and D. Richter, Cooperative chain dynamics of tracer chains in highly entangled polyethylene melts, Phys. Rev. Lett. **126**, 187801 (2021).
[21] A. Wischnewski, M. Monkenbusch, L. Willner, D. Richter, and G. Kali, Direct observation of the transition from free to constrained single-segment motion in entangled polymer melts, Phys. Rev. Lett. **90**, 058302 (2003).
[22] M. Guenza, Intermolecular effects in the center-of-mass dynamics of unentangled polymer fluids, Macromolecules **35**, 2714 (2002).
[23] D. Richter, M. Monkenbusch, A. Arbe, and J. Colmenero, *Neutron Spin Echo in Polymer Systems* (Springer, Berlin, Heidelberg, 2005), Vol. 174, 10.1007/b106578.
[24] M. Kruteva, J. Allgaier, I. Hoffmann, M. Monkenbusch , and D. Richter, Unravelling the relevant modes behind the cooperative dynamics in highly entangled polymer melts, Institut Laue-Langevin (ILL) (2024), 10.5291/ILL-DATA.9-11-2148.
[25] B. Farago, P. Falus, I. Hoffmann, M. Gradzielski, F. Thomas, and C. Gomez, The IN15 upgrade, Neutron News **26**, 15 (2015).
[26] M. Monkenbusch, M. Kruteva, and D. Richter, Dynamic structure factors of polymer melts as observed by neutron spin echo: Direct comparison and reevaluation, J. Chem. Phys. **159**, 034902 (2023).
[27] The difference between N_e values derived from macroscopic rheology experiments and microscopic NSE measurements is a general finding. For all investigated polymers by NSE N_e is found to be about 40% larger than the rheological result (see, e.g., Ref. [26]). We might add the chain confinement in NSE is directly observed as the Fourier transformed of the reptation tube. Apparently, the microscopic confinement observed by NSE is weaker than that derived from rheo-theories.

Correction: The author names in Ref. [24] were presented incorrectly and have been fixed.